Polymer 50 (2009) 3822–3827

Contents lists available at ScienceDirect

Polymer

journal homepage: www.elsevier.com/locate/polymer

Transition behavior and ionic conductivity of lithium perchlorate-doped polystyrene-*b*-poly(2-vinylpyridine)

Bokyung Kim [a], Hyungju Ahn [a], Jong Hak Kim [a], Du Yeol Ryu [a,*], Jehan Kim [b]

[a] Department of Chemical and Biomolecular Engineering, Yonsei University, 134 Shinchon-dong, Seodaemun-gu, Seoul 120-749, Republic of Korea
[b] Beamline Department, Pohang Accelerator Laboratory, Pohang 790-784, Republic of Korea

ARTICLE INFO

Article history:
Received 16 February 2009
Received in revised form
12 April 2009
Accepted 13 May 2009
Available online 22 May 2009

Keywords:
Block copolymers
Transition behavior
Ionic conductivity

ABSTRACT

We report the transition behavior and the ionic conductivity of ion-doped amorphous block copolymer, based on two compositionally different polystyrene-*block*-poly(2-vinylpyridine) copolymers (PS-*b*-P2VPs) that can self-assemble into nanostructures, where P2VP block is ionophilic to lithium perchlorate ($LiClO_4$). The transition temperatures of $LiClO_4$-doped PS-*b*-P2VP, like the order-to-disorder transition (T_{ODT}), were measured by small-angle X-ray scattering (SAXS) and depolarized light scattering (DPLS). The selective ionic coordination to the nitrogen units of P2VP block leads to the increase of the repulsive interactions between two block components from weak- to strong-segregation regime with increasing amount of $LiClO_4$, which results subsequently in the increased T_{ODT}. However, for a compositionally asymmetric PS-*b*-P2VP under lamellar morphology, the ionic conductivity by the addition of $LiClO_4$ was remarkably increased at higher temperatures, representing that the effective ionic coordination at the greater volume fraction of P2VP block component improves the ionic conductivity as the temperature approaches to a rubbery phase.

1. Introduction

Polymer electrolytes have recently attracted attention as promising solid-state materials for electrochemical devices such as rechargeable lithium batteries, fuel cells, and dye-sensitized solar cells [1–10]. Polymeric materials allow the safety in use and the facile process in manufacture compared with most liquid electrolytes, while there are still two competing electrical and mechanical requirements for the best performance [1–8]. Some research efforts have been focused on the design of ion-doped polymer electrolytes which constitute the coordination in the host polymers with the alkali metal salts so as to induce the selective miscibility in the molecular level and enhance the ionic conductivity [11,12]. Hence, the search for new systems in the polymer electrolytes has continued to look for a desirable performance between high ionic conductivity and good physical stability.

Recently, block copolymer (BCP) has been used in the fields of polymer electrolytes as an attractive material to achieving the ionic conductivity and mechanical stability simultaneously [13–22]. A diblock copolymer consisting of two chemically dissimilar polymers, covalently linked together at one end, can self-assemble in tens of nanometers into periodically ordered arrays depending on the volume fraction of the blocks; for examples, lamellar, cylindrical, gyroid, and spherical microdomains. This approach allows us indeed to incorporate higher ionic properties into a polymer material while retaining desirable mechanical properties to resist to flow due to the nanostructured self-assembly of BCP. The microphase separation generally occurs provided the product χN is sufficiently large ($\chi N >> 10.5$ in the case of symmetric BCP), where χ is the segmental interaction parameter and N is the total number of segments in the BCP [23–25]. When χ, therefore, is inversely proportional to temperature (T), a phase-mixed (disordered) state at elevated temperature can be obtained, while microphase-separating upon cooling. This transition from the ordered to the disordered state, denoted as T_{ODT}, occurs when the unfavorable segmental interactions are sufficiently weakened and the entropy of mixing in two block components dominates, characterized by a solid-like to liquid-like behavior in rheological response [23,24].

The self-assembled BCP electrolytes involving poly(ethylene-oxide) (PEO) and poly(vinylpyridine) (PVP) have been studied since they enable PEO or PVP block to form coordinative structures with the alkali metal salts to elevate the ionic conductivity, where the other block supports dimensional stability [18–21]. Especially for PEO-based electrolytes, it has been a key issue to inhibit crystallization which causes diminishing the ionic conductivity [18,19].

* Corresponding author. Tel.: +82 2 2123 5756; fax: +82 2 312 6401.
E-mail address: dyryu@yonsei.ac.kr (D.Y. Ryu).

0032-3861/$ – see front matter © 2009 Elsevier Ltd. All rights reserved.
doi:10.1016/j.polymer.2009.05.022

In this study, we investigate the transition behavior and the ionic conductivity of amorphous BCP electrolyte composed of a polystyrene-*block*-poly(2-vinylpyridine) (PS-*b*-P2VP) and lithium perchlorate ($LiClO_4$) that is selectively coordinated to the ionophilic P2VP block. The phase behavior for two compositionally different lamellar-forming PS-*b*-P2VPs represents by small-angle X-ray scattering (SAXS) that the addition of $LiClO_4$ enhances the microphase separation from weak- to strong-segregation regime. Moreover, the compositional asymmetry in PS-*b*-P2VP with $LiClO_4$ leads to the significant improvement in the ionic conductivity with increasing temperature while holding the same lamellar morphology. This result can be correlated to the facile ionic transport in asymmetric PS-*b*-P2VP due to the greater volume fraction of P2VP block component.

2. Experimental section

2.1. Materials

Two compositionally different BCPs, PS-*b*-P2VP, were synthesized by the sequential, anionic polymerization of styrene and 2-vinylpyridine in tetrahydrofuran (THF) at −78 °C under purified argon environment using *sec*-butyllithium as an initiator. Refluxed THF from CaH_2 was stirred over fresh sodium-benzophenone complex until it showed a deep purple color indicating an oxygen- and moisture-free solvent. Degassed monomers with CaH_2, styrene and 2-vinylpyridine (Aldrich), were vacuum distilled over dried dibutyl magnesium and trioctyl aluminum, respectively, until a persistent characteristic color was observed. The polymer solution terminated with purified 2-propanol was precipitated in excess hexane. The absolute weight- and number-average molecular weights (M_w and M_n) and polydispersity (M_w/M_n) were measured by size-exclusion chromatography (SEC) and PS volume fraction (f_{PS}) of PS-*b*-P2VP was determined by ^1H nuclear magnetic resonance (^1H NMR) with mass densities of two components (1.05 and 1.14 g/cm^2 for PS and P2VP, respectively), as listed in Table 1.

PS-*b*-P2VP electrolytes with various amounts of lithium perchlorate ($LiClO_4$) were prepared by freeze-drying method with benzene. For instance, a predetermined amount of PS-*b*-P2VP and $LiClO_4$ was dissolved in benzene (~8 wt% in solute) and ethanol, respectively, and the quenched solution was evaporated under vacuum for 24 h, followed by sequential annealing for 3 days to thermally equilibrate the sample and to remove the solvent completely. The molar ratio of $LiClO_4$ to 2-vinylpyridine (2VP) in the PS-*b*-P2VP, denoted as $X = [LiClO_4]/[2VP]$, was varied up to approximately 0.1.

2.2. Small-angle X-ray scattering (SAXS)

The transition temperatures for the samples were measured by the synchrotron SAXS, which were performed in 4C1 beamline at the Pohang Light Source (PLS), Korea [26]. The operating conditions were set to a wavelength of 1.608 Å ($\Delta\lambda/\lambda = 1.5 \times 10^{-2}$), the sample-to-detector distance of 2 m, the beam size of 1×1 mm^2, and the sample thickness of 1.5 mm. A 2D-CCD detector (Princeton Instruments Ins., SCX-TE/CCD-1242) was used to collect the scattered X-rays. A home-made heating cell was used for temperature sweep experiment at constant heating rate 0.9 °C/min from 150 to 260 °C, and all the experiments were carried out under the nitrogen flow in order to avoid thermal degradation of the polymer samples. The exposure time for all measurements was 60–120 s.

Table 1
Molecular characteristics of block copolymers in this study.

Specimen	M_n[a]	M_w/M_n[a]	f_{PS}[b]	State
PS-*b*-P2VP-01	15,100	1.05	0.504	Lamella to disorder at $T_{ODT} = 162$ °C
PS-*b*-P2VP-02	21,100	1.04	0.381	Lamella to disorder at $T_{ODT} = 164$ °C

[a] Weight- and number-average molecular weights (M_w and M_n) and polydispersity (M_w/M_n) were measured by size-exclusion chromatography (SEC).
[b] Volume fraction of PS for PS-*b*-P2VP was measured by ^1H nuclear magnetic resonance (NMR) with mass densities of two components (1.05 and 1.14 g/cm^3 for PS and P2VP, respectively).

2.3. Fourier-transform infrared spectroscopy (FT-IR)

FT-IR spectra (Bruker Tensor 27, Germany) were used to measure the interaction between the nitrogen units of P2VP block and $LiClO_4$ at room temperature. The typical wavenumber scan ranges of 4000–400 cm^{-1} with the scan number of 32 and the spectral resolution of 4 cm^{-1}. The dried samples were physically mixed with potassium bromide (KBr) and pressed to a disk before measurements.

2.4. AC impedance

The ionic conductivity (σ) of PS-*b*-P2VP electrolytes was measured by a AC impedance analyzer (IM6e, ZAHNER, Germany) using lab-made four-probe Teflon cell equipped with a temperature controller, which is operated over frequency range form 1 MHz to 1 Hz in galvanostatic mode under AC current amplitude of 0.01 mA. σ (in S/cm) is calculated by $\sigma = L/R \times S$, where L (in cm), R (in Ω), and S (in cm^2) are the distance between the electrodes, the impedance, and the surface area for ions to penetrate the polymer electrolyte, respectively [27]. All the dried sample disks at 1.0 mm thick were prepared right before measurements in order to avoid the influence of moisture, with the data being reproducible.

3. Results and discussion

An ion-doped polymer electrolyte is designed within the concepts of self-assembled BCP nanostructures, composed of amorphous PS-*b*-P2VP and $LiClO_4$, where P2VP block is selectively ionophilic. To ensure whether the ionic coordination takes place between $LiClO_4$ and the nitrogen units of 2VP within ion-doped PS-*b*-P2VP electrolytes, FT-IR spectra were measured for $LiClO_4$-doped PS-*b*-P2VP, as shown in Fig. 1 at selected wavenumber (ν) range from 1650 to1325 cm^{-1}. FT-IR absorbance spectrum for PS-*b*-P2VP-01 with no $LiClO_4$ shows the characteristic peaks due to phenyl ring stretching at $\nu = 1600$, 1493, and 1452 cm^{-1}, and pyridine ring stretching at $\nu = 1589$, 1473, and 1433 cm^{-1}, respectively [15,28–30] In contrast to no peak shift in phenyl ring stretching, for $LiClO_4$-doped PS-*b*-P2VP-01, three peaks due to pyridine ring stretching are shifted toward higher ν in proportion to the amount of $LiClO_4$, leading to $\nu = 1595$, 1476, and 1435 cm^{-1} for the molar ratio (X) of $[LiClO_4]/[2VP] = 0.092$, respectively. This can be attributed to the attractive ionic coordination of Li^+ to the nitrogen units of 2VP (hereafter denoted as the ionic coordination), representing that the degree of ionic coordination per 2VP increases with increasing X [11,12]. The similar data of FT-IR spectra were observed for $LiClO_4$-doped PS-*b*-P2VP-02 (data not shown).

Fig. 2(a) shows SAXS intensity profiles for $LiClO_4$-doped PS-*b*-P2VP-01 of $X = 0.015$, measured at various temperatures from 151 to 247 °C during heating at a heating rate of 0.9 °C/min, as a function of the scattering vector (q), where $q = (4\pi/\lambda)\sin\theta$, 2θ and λ are the scattering angle and wavelength, respectively. At low temperatures ($T < 208$ °C), a strong and sharp scattering peak located at $q = 0.43$ nm^{-1} is observed, indicative of the microphase separation due to the unfavorable segmental interactions between two block components. No higher-order peak relative to the first-order

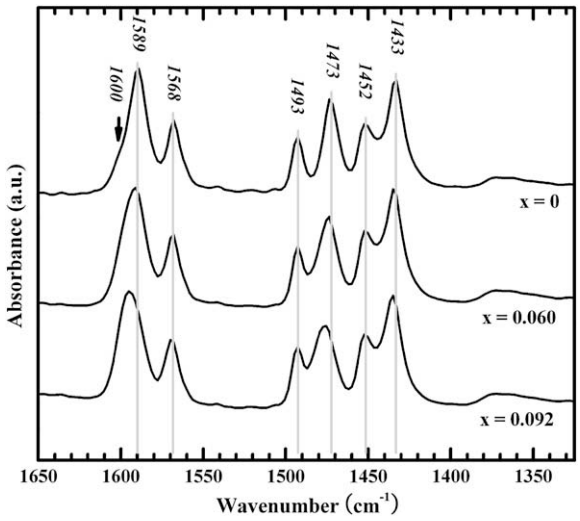

Fig. 1. FT-IR absorbance spectra for PS-*b*-P2VP-01 and $LiClO_4$-doped PS-*b*-P2VP-01 of $X = 0.060, 0.092$, where X denotes the molar ratio of $[LiClO_4]/[2VP]$. Three peaks due to pyridine ring stretching at $\nu = 1589$, 1473, and 1433 cm^{-1} are significantly shifted toward higher ν in proportion to the amount of $LiClO_4$.

reflection represents the low contrast in electron densities between two components. Keeping in mind that PS-*b*-P2VP-01 is symmetrically composed of PS and P2VP ($f_{PS} = 0.504$), it should correspond to lamellar microdomain morphology. With increasing temperature for $T > 208$ °C, the primary peak weakens and broadens significantly, then maintains a diffuse maximum, which arises from the correlation hole scattering of a phase-mixed (or disordered) BCP. This behavior is typical for BCPs undergoing a transition from the ordered to disordered state with temperature. Accordingly, one can readily determine a order-to-disorder transition (T_{ODT}) at 208 °C for $LiClO_4$-doped PS-*b*-P2VP-01 of $X = 0.015$ by the discontinuous changes of the scattering parameters derived from the SAXS profiles, like the inverse of the maximum intensity ($1/I(q^*)$), full-width at half-maximum (FWHM), and *d*-spacing (d) by $d = 2\pi/q^*$ as a function of inverse temperature (1/K), as plotted in Fig. 2(b). As temperature increases over T_{ODT}, $1/I(q^*)$ and FWHM remarkably increase because the interaction parameter (χ) between two components decreases proportionally to $1/T$ and the thermal fluctuation increases, while *d*-spacing with a discontinuity at T_{ODT} gradually decreases for $T > T_{ODT}$, as a characteristic length scale of the radius of gyration (R_g) by thermal fluctuation in composition. This type of temperature dependence of *d*-spacing at disordered state was reported by several studies [31–34], which are inconsistent with the mean-field argument [25,35] where *d*-spacing at disordered state is independent of $1/T$. For comparison, the other for PS-*b*-P2VP-01 with no $LiClO_4$ is determined in the similar manner at $T_{ODT} = 162$ °C, indicating that a very small amount of $LiClO_4$ ($X = 0.015$) in PS-*b*-P2VP-01 efficiently elevates T_{ODT} by 46 °C.

Fig. 3 shows transition temperatures for $LiClO_4$-doped PS-*b*-P2VP-01 and PS-*b*-P2VP-02, evaluated by SAXS and depolarized light scattering (DPLS), as a function of $X = [LiClO_4]/[2VP]$. Here, the original T_{ODT} for asymmetric PS-*b*-P2VP-02 was measured to be 164 °C, as determined by SAXS. With increasing amount of $LiClO_4$ in PS-*b*-P2VP, the T_{ODT} increases up to the degradation temperature ($T_d \approx 250$ °C) in this study, regardless of the block composition between PS-*b*-P2VP-01 and PS-*b*-P2VP-02. An increase of T_{ODT} with increasing amount of $LiClO_4$ (2350 °C/molar ratio) is comparable to the results (2000 °C/molar ratio) for $CdCl_2$-coordinated PS-*b*-P2VP [36,37]. This can be correlated to the enhancement of ordered phase by the selective ionic coordination to the nitrogen units of

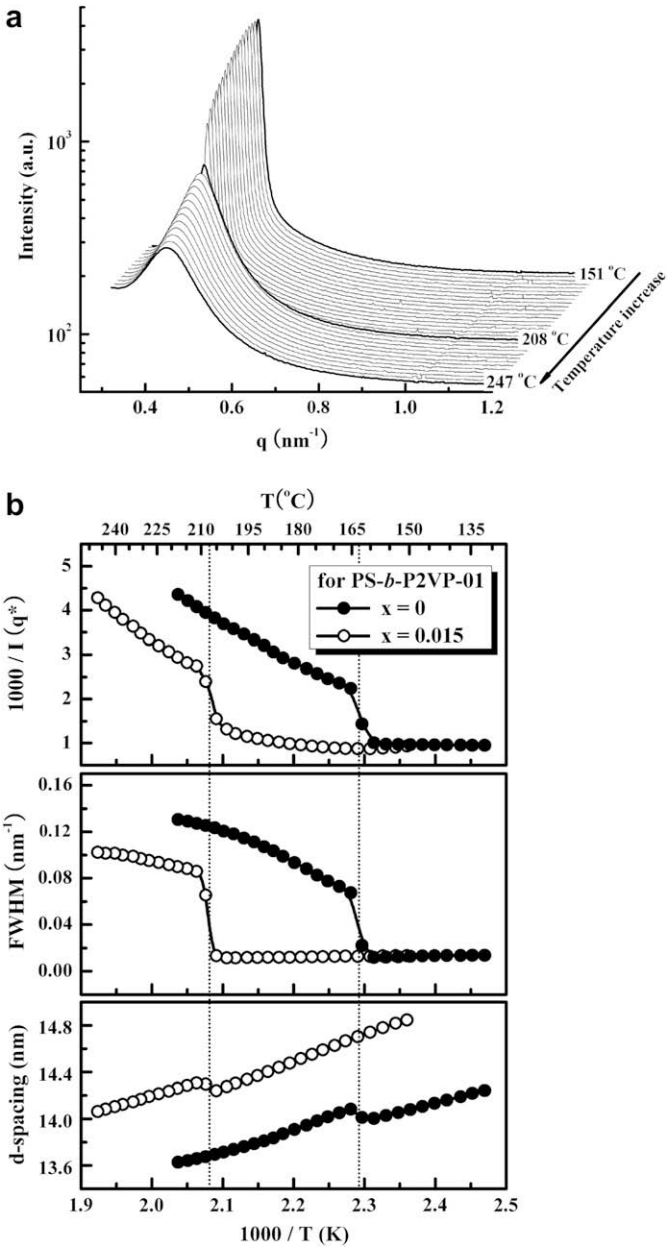

Fig. 2. (a) SAXS intensity profiles for $LiClO_4$-doped PS-*b*-P2VP-01 of $X = 0.015$ as a function of the scattering vector (q), which were measured at various temperatures during heating at a heating rate of 0.9 °C/min from 151 to 247 °C, and (b) the scattering parameters for PS-*b*-P2VP-01 and $LiClO_4$-doped PS-*b*-P2VP-01 of $X = 0.015$. The inverse of the maximum intensity ($1/I(q^*)$), full-width at half-maximum (FWHM), and *d*-spacing (d) by $d = 2\pi/q^*$ are plotted as a function of inverse temperature (1/K).

P2VP block, which will lead to the increase of the repulsive interactions between two block components from weak- to strong-segregation regime.

To elucidate the relevant phase morphology for $LiClO_4$-doped PS-*b*-P2VP, we measured SAXS intensity profiles at the various amount of $LiClO_4$ after annealing at 150 °C, as shown in Fig. 4. As the molar ratio (X) increases, the higher-order scattering peaks become evident, confirming the enhanced ordering degree in BCP self-assembly, which is desirable in ion-doped BCP electrolytes to avoid ionic trap at interfaces. For both $LiClO_4$-doped PS-*b*-P2VP-01 and PS-*b*-P2VP-02 of $X = \sim 0.09$, it is distinctly seen that the microphase corresponds to a lamellar structure, evidenced by a sharp scattering peak and the higher-order peaks (indicated by arrows) at scattering

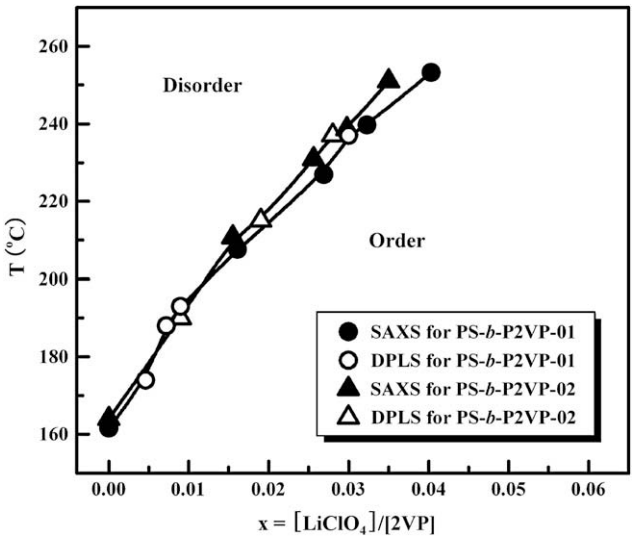

Fig. 3. Order-to-disorder transition temperatures (T_{ODT}) for $LiClO_4$-doped PS-*b*-P2VP-01 and PS-*b*-P2VP-02, evaluated by SAXS and depolarized light scattering (DPLS), as a function of $X = [LiClO_4]/[2VP]$. The linear least-squares fit to T_{ODT} yields 2350 °C/molar ratio (X), and the degradation temperature (T_d) was set to be 250 °C in this study.

vector ratios of $q/q^* = 1: 2: 3$ relative to a primary peak located at q^* (at maximum). It is also worthwhile to note that at $X = \sim 0.09$, symmetric PS-*b*-P2VP-01 exhibits weaker second-peak due to the destructive scattering interferences in comparison to that of asymmetric PS-*b*-P2VP-02.

A prominent shift toward lower q^* with increasing X to be ~0.09, derived from the SAXS profiles in Fig. 4, indicates an increase in *d*-spacing (or inter-lamellar spacing) by ~20%, as illustrated in Fig. 5(a) as a function of $X = [LiClO_4]/[2VP]$. It can be a consequence of the increase of the repulsive interactions between two block components by the ionic coordination to the nitrogen units of P2VP block, as mentioned above. However, it is of great interest for such an asymmetric PS-*b*-P2VP electrolyte that $LiClO_4$-doped PS-*b*-P2VP-02 maintains a lamellar morphology, although *d*-spacing increases up to ~20% with increasing amount of $LiClO_4$. Provided that the volume fraction of P2VP block component with $LiClO_4$ increases, this is more than likely because the phase transformation to cylindrical or the other morphologies is restricted, which is caused by the multiple ionic coordinations with more than single nitrogen unit of P2VP block [38], consequently persisting in the same lamellar morphology. FWHM for $LiClO_4$-doped PS-*b*-P2VP, as shown in Fig. 5(b), indicates that the ordering degree in BCP self-assembly by the addition of $LiClO_4$ is more enhanced for asymmetric PS-*b*-P2VP-02 presumably due to the effective ionic coordination at greater volume fraction of P2VP block component, while similar for symmetric PS-*b*-P2VP-01 with increasing X. The results presented here, hence, further illustrate how PS-*b*-P2VP might be applied to design ion-doped BCP electrolytes that can self-assemble into nanostructures by allowing the selective ionic coordination.

Fig. 6 shows ionic conductivities for $LiClO_4$-doped PS-*b*-P2VP electrolytes, measured using a galvanostatic four-probe method as a function of inverse temperature (1/K) from 110 to 30 °C, which are lower than T_{ODT} for both $LiClO_4$-doped PS-*b*-P2VP-01 and PS-*b*-P2VP-02. The ionic conductivity determined by four-probe method might be higher to some degree but more accurate than that by two-probe method due to the minimization of contact impedance. The improved conductivities with increasing temperature are in general responsible for the increased polymer chain mobility favoring the facile ionic transport. At higher temperatures ($T = \sim 100$ °C) for PS-*b*-P2VP-02, remarkable improvement in conductivities by the addition of $LiClO_4$ indeed suggests that the

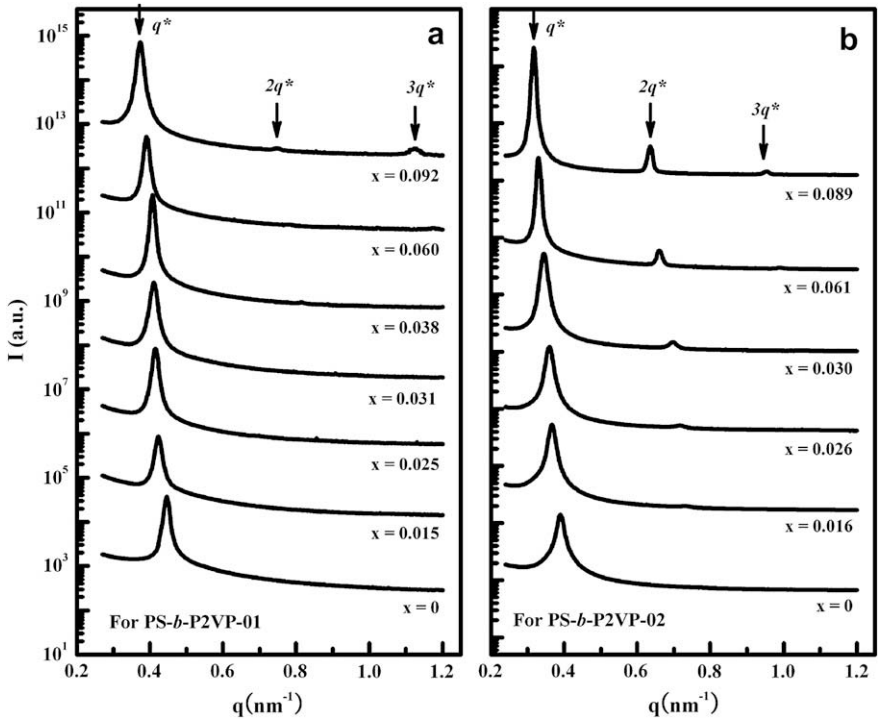

Fig. 4. SAXS intensity profiles at the various amount of $LiClO_4$ after annealing at 150 °C for (a) $LiClO_4$-doped PS-*b*-P2VP-01 and (b) $LiClO_4$-doped PS-*b*-P2VP-02, where X denotes the molar ratio of $[LiClO_4]/[2VP]$. A sharp scattering peak and the higher-order peaks at scattering vector ratios of $q/q^* = 1: 2: 3$ relative to a maximum q^* correspond to a lamellar structure, as indicated by arrows.

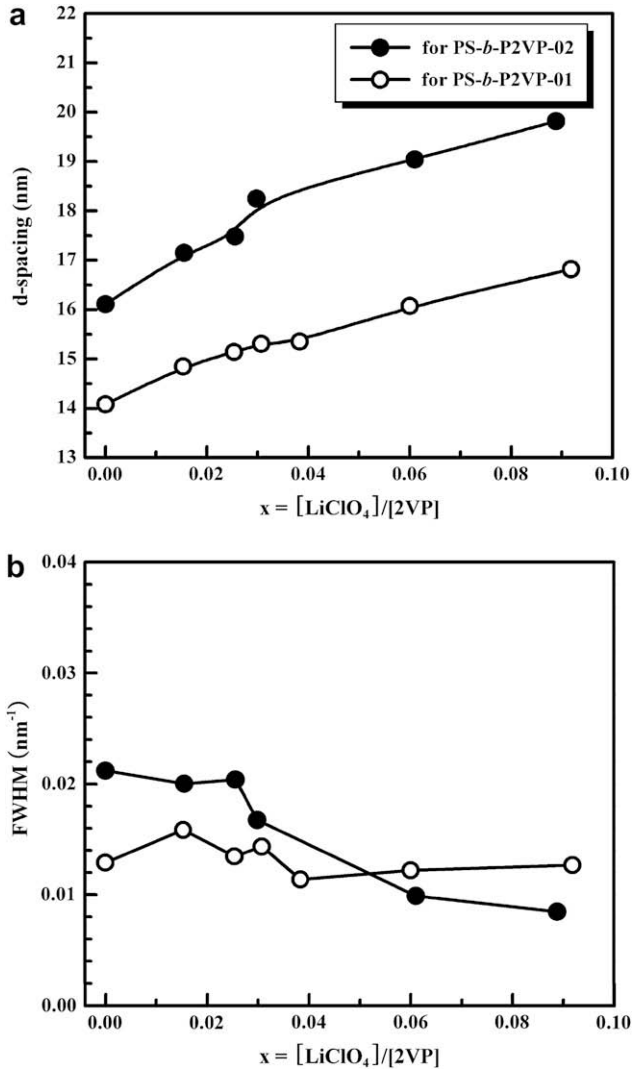

Fig. 5. (a) *d*-Spacing (or inter-lamellar spacing), and (b) full-width at half-maximum (FWHM) for $LiClO_4$-doped PS-*b*-P2VP as a function of $X = [LiClO_4]/[2VP]$, which were derived from the SAXS profiles in Fig. 4.

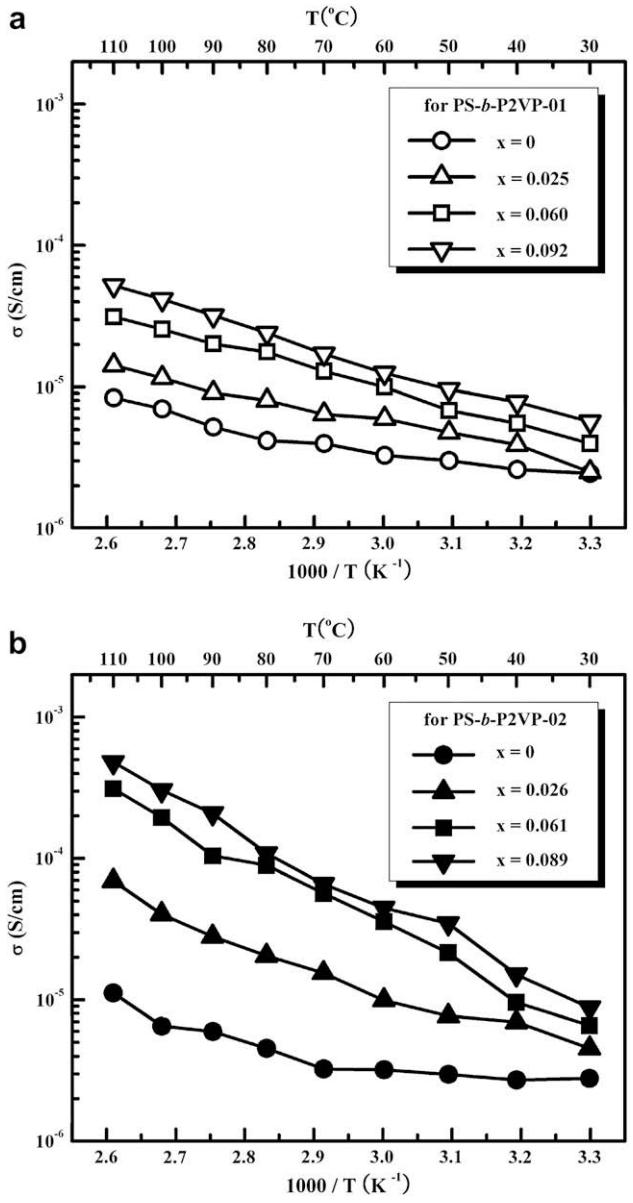

Fig. 6. Ionic conductivity (σ) for (a) $LiClO_4$-doped PS-*b*-P2VP-01 and (b) $LiClO_4$-doped PS-*b*-P2VP-02, as a function of inverse temperature (1/K) from 110 to 30 °C, where the molar ratio of $[LiClO_4]/[2VP]$ was varied up to $X = \sim 0.09$.

ionic mobility can be enhanced for asymmetric PS-*b*-P2VP as long as the same lamellar morphology remains unchanged. Using a typical Arrhenius temperature dependence, the ionic conductivity can be analyzed, $\sigma = \sigma_o \exp(-E_a/RT)$, where σ_o is the conductivity in the limit of infinite temperature and E_a is an apparent activation energy to overcome energy barrier, which are available from the linear least-squares fit to logarithmic σ, yielding an intercept at *x*-axis and a slope corresponding σ_o to and E_a, respectively. With increasing amount of $LiClO_4$, a significant increase of E_a for $LiClO_4$-doped PS-*b*-P2VP-02 was observed compared to that for $LiClO_4$-doped PS-*b*-P2VP-01, as would be expected by the slope change. This can also be attributed to the effective ionic coordination at greater volume fraction of P2VP block component for $LiClO_4$-doped PS-*b*-P2VP-02, leading to the decreased chain mobility. However, the improved conductivities at higher temperatures ($T = \sim 100$ °C) represent that the ionic conductivity can be efficiently enhanced by plasticizing $LiClO_4$-doped PS-*b*-P2VP. In fact, the ion-doped BCP may offer the desirable properties for solid-state polymer electrolytes when it controlled optimally because of its great versatility to improve the ionic conductivity through a continuous random orientation of the closely connected grains consisting of lamellar microdomains. Thus, this demonstrates that within the same lamellar morphology for $LiClO_4$-doped PS-*b*-P2VP, the block composition should be taken into consideration for the best electrical performance.

4. Conclusion

The transition behavior and ionic conductivity of $LiClO_4$-doped PS-*b*-P2VP was investigated as an ion-doped BCP electrolyte system that can self-assemble into nanostructures. As evidenced by SAXS results, the ionic coordination to the nitrogen units of P2VP enhances the ordered phase, resulting in an increase of T_{ODT} and *d*-spacing with increasing amount of $LiClO_4$, which is caused by the increase of the repulsive interactions between two block components. The ordered morphology was turned out to be a lamellar microdomain by SAXS intensity profiles, regardless of block compositions between PS-*b*-P2VP-01 ($f_{PS} = 0.504$) and PS-*b*-P2VP-02 ($f_{PS} = 0.381$). This allows us to speculate that for asymmetric

PS-*b*-P2VP-02 the multiple ionic coordinations with more than single nitrogen unit of P2VP block restrict the phase transformation, hence, persisting in the same lamellar morphology even at the increased volume fraction of $LiClO_4$-coordinated P2VP block component. Especially for asymmetric PS-*b*-P2VP-02, the ionic conductivity by the addition of $LiClO_4$ was remarkably increased at higher temperatures, representing that the effective ionic coordination at the greater volume fraction of P2VP block component improves the ionic conductivity as the temperature approaches to a rubbery phase. This study shows that an ion-doped PS-*b*-P2VP electrolyte can lead possibly to another accessible route to new solid-state BCP electrolytes.

Acknowledgement

This work was supported by the Nuclear R&D Programs and APCPI ERC program (R11-2007-050-02001) funded by the Ministry of Education, Science & Technology (MEST), Korea.

References

[1] Tarascon JM, Armand M. Nature 2001;414:359.
[2] Patil A, Patil V, Shin DW, Choi JW, Paik DS, Yoon SJ. Mater Res Bull 2008; 43:1913.
[3] Agrawal RC, Pandey GP. J Phys D Appl Phys 2008;41:223001.
[4] Stephan AM. Eur Polym J 2006;42:21.
[5] Ratner MA, Shriver DF. Chem Rev 1988;88:109.
[6] Stephan AM, Nahm KS. Polymer 2006;47:5952.
[7] Langsdorf BL, Sultan J, Pickup PG. J Phys Chem B 2003;107:8412.
[8] Stergiopoulos T, Arabatzis IM, Katsaros G, Falaras P. Nano Lett 2002;2:1259.
[9] Angell CA, Xu K, Zhang SS, Videa M. Solid State Ionics 1996;86–88(Part 1):17.
[10] Chiu CY, Yen YJ, Kuo SW, Chen HW, Chang FC. Polymer 2007;48:1329.
[11] Li J, Khan IM. Macromolecules 1993;26:4544.
[12] Li J, Mintz EA, Khan IM. Chem Mater 1992;4:1131.
[13] Soo PP, Huang B, Jang YI, Chiang YM, Sadoway DR, Mayes AM. J Electrochem Soc 1999;146:32.
[14] Ruzette AVG, Soo PP, Sadoway DR, Mayes AM. J Electrochem Soc 2001; 148:A537.
[15] Kosonen H, Valkama S, Hartikainen J, Eerikainen H, Torkkeli M, Jokela K, et al. Macromolecules 2002;35:10149.
[16] Higa M, Fujino Y, Koumoto T, Kitani R, Egashira S. Electrochim Acta 2005; 50:3832.
[17] Ryu SW, Trapa PE, Olugebefola SC, Gonzalez-Leon JA, Sadoway DR, Mayes AM. J Electrochem Soc 2005;152:A158.
[18] Chiu CY, Hsu WH, Yen YJ, Kuo SW, Chang FC. Macromolecules 2005;38: 6640.
[19] Guilherme LA, Borges RS, Moraes EMS, Silva GG, Pimenta MA, Marletta A, et al. Electrochim Acta 2007;53:1503.
[20] Li J, Kamata K, Komura M, Yamada T, Yoshida H, Iyoda T. Macromolecules 2007;40:8125.
[21] Bronstein LM, Karlinsey RL, Yi Z, Carini J, Werner-Zwanziger U, Konarev PV, et al. Chem Mater 2007;19:6258.
[22] Ioannou EF, Mountrichas G, Pispas S, Kamitsos EI, Floudas G. Macromolecules 2008;41:6183.
[23] Hashimoto T. Thermoplastic elastomers. New York: Hanser; 1987.
[24] Bate FS, Fredrickson G. Ann Rev Phys Chem 1990;41:525.
[25] Leibler L. Macromolecules 1980;13:1602.
[26] Yoon J, Kim KW, Kim J, Heo K, Jin KS, Jin S, et al. Macromol Res 2008; 16:575.
[27] Park JT, Lee KJ, Kang MS, Kang YS, Kim JH. J Appl Polym Sci 2007;106:4083.
[28] Li XD, Goh SH. Polymer 2002;43:6853.
[29] Kuo SW, Wu CH, Chang FC. Macromolecules 2004;37:192.
[30] Kim HJ, Kim SB, Kim JK, Jung YM, Ryu DY, Lavery KA, et al. Macromolecules 2006;39:408.
[31] Rosedale JH, Bates FS, Almdal K, Mortensen K, Wignall GD. Macromolecules 1995;28:1429.
[32] Sakamoto N, Hashimoto T. Macromolecules 1995;28:6825.
[33] Bodycomb J, Yamaguchi D, Hashimoto T. Macromolecules 2000;33:5187.
[34] Corvazier L, Messe L, Salou CLO, Young RN, Fairclough JPA, Ryan AJ. J Mater Chem 2001;11:2864.
[35] Mori K, Hasegawa H, Hashimoto T. Polymer 2001;42:3009.
[36] Lee DH, Kim HY, Kim JK, Huh J, Ryu DY. Macromolecules 2006;39:2027.
[37] Lee DH, Han SH, Joo W, Kim JK, Huh J. Macromolecules 2008;41:2577.
[38] Atorngitjawat P, Runt J. J Phys Chem 2007;111:13483.